



**A Novel Liquid Biopsy-Based Approach for Highly Specific
Cancer Diagnostics: Mitigating False Responses in Assaying
Patient Plasma-Derived Circulating microRNAs through
Combined SERS and Plasmon-Enhanced Fluorescence
Analyses**

Journal:	<i>Analyst</i>
Manuscript ID	AN-ART-03-2020-000538.R1
Article Type:	Paper
Date Submitted by the Author:	20-May-2020
Complete List of Authors:	Masterson, Adrianna; Indiana University Purdue University Indianapolis, Chemistry and Chemical Biology Liyanage, Thakshila; Indiana University Purdue University Indianapolis, Department of Chemistry and Chemical Biology Berman, Claire; Indiana University Purdue University Indianapolis, Chemistry and Chemical Biology Kaimakliotis, Hristos; Indiana University Purdue University Indianapolis, Chemistry and Chemical Biology Johnson, Merrell; Purdue University Fort Wayne, Department of Physics Sardar, Rajesh; Indiana University Purdue University Indianapolis, Chemistry and Chemical Biology

1
2
3 **A Novel Liquid Biopsy-Based Approach for Highly Specific Cancer**
4 **Diagnostics: Mitigating False Responses in Assaying Patient Plasma-Derived**
5 **Circulating microRNAs through Combined SERS and Plasmon-Enhanced**
6 **Fluorescence Analyses**
7
8
9
10

11
12 Adrianna N. Masterson,^{a,#} Thakshila Liyanage,^{a,#} Claire Berman,^a Hristos Kaimakliotis,^b Merrell
13
14 Johnson,^c and Rajesh Sardar^{*,a,s}
15
16

17 ^aDepartment of Chemistry & Chemical Biology, Indiana University-Purdue University
18 Indianapolis, 402 N. Blackford Street, Indianapolis, Indiana 46202, United States
19

20 ^bDepartment of Urology, Indiana University School of Medicine, 535 N. Barnhill Dr.
21 Indianapolis, Indiana 46202, United States
22
23

24 ^cDepartment of Physics, Purdue University Fort Wayne, 2101 E. Coliseum Blvd.
25 Fort Wayne, Indiana 46805, United States
26

27 ^sIntegrated Nanosystems Development Institute, Indiana University-Purdue University
28 Indianapolis, 723 W. Michigan Street, Indianapolis, Indiana 46202, United States
29
30

31
32
33 [#]These authors contributed equally to this work.
34
35

36 **KEYWORDS:** surface enhanced Raman scattering, plasmon-enhanced fluorescence, multimodal
37
38 assay, microRNAs, gold triangular nanoprisms, liquid biopsy, point-of-care diagnostic
39
40
41
42
43
44
45
46
47
48
49
50
51
52
53
54
55
56
57
58
59
60

1
2
3 **One sentence text:** Novel multimodal assay has been developed to quantify circulating
4 microRNAs through a combined surface-enhanced Raman scattering and plasmon-enhanced
5 fluorescence approach
6
7
8
9
10

11 **Abstract:**
12

13
14 Studies have shown that microRNAs, which are small noncoding RNAs, hold tremendous
15 promise as next-generation circulating biomarkers for early cancer detection via liquid biopsies.
16 A novel, solid-state nanoplasmonic sensor capable of assaying circulating microRNAs through a
17 combined surface-enhanced Raman scattering (SERS) and plasmon-enhanced fluorescence
18 (PEF) approach has been developed. Here, the unique localized surface plasmon resonance
19 properties of chemically-synthesized gold triangular nanoprisms (Au TNPs) are utilized to create
20 large SERS and PEF enhancements. With careful modification to the surface of Au TNPs, this
21 sensing approach is capable of quantifying circulating microRNAs at femtogram/microliter
22 concentrations. Uniquely, the multimodal analytical methods mitigate both false positive and
23 false negative responses and demonstrate the high stability of our sensors within bodily fluids.
24 As a proof of concept, microRNA-10b and microRNA-96 were directly assayed from the plasma
25 of six bladder cancer patients. Results show potential for a highly specific liquid biopsy method
26 that could be used in point-of-care clinical diagnostics to increase early cancer detection or any
27 other diseases including SARS-CoV-2 in which RNAs can be used as biomarkers.
28
29
30
31
32
33
34
35
36
37
38
39
40
41
42
43
44
45
46
47
48
49
50
51
52
53
54
55
56
57
58
59
60

Introduction

Liquid biopsies involve analyzing circulating biomolecules in bodily fluids provide many advantages over traditional tissue biopsies for detecting cancers at an early stage as they are non-invasive, less expensive, and simpler.¹ Small non-coding RNAs, known as microRNAs, have been found to regulate a large number of human genes and play a significant role in various cancer developments.²⁻⁷ Many studies have demonstrated that the detection of circulating microRNAs at an early stage, via liquid biopsies, could allow better treatment in an effort to prevent cancer progression and metastasis, increasing the chance of patient survival. The current “gold-standard” microRNA assays (i.e., quantitative reverse-transcription polymerase chain reaction (qRT-PCR)-based technologies) are capable of measuring microRNA levels reproducibly from bodily fluids in real-life clinical samples. However, this technology has several drawbacks including: (1) the treatment of biological fluid, (2) complicated labor-intensive RNA extraction, (3) required labeling and amplification prior to analysis, (4) complementary DNA conversion steps, and (5) the large volume of patient samples needed.⁸ Together, these traits hinder translation into clinical point-of-care (POC) diagnostics.

In contrast, solid-state, label-free biosensing offers many unique advantages over qRT-PCR techniques, including simple sensor fabrication, high sensitivity, easy to miniaturization (of particular importance when adapting technologies to POC diagnostics), and elimination of receptor tagging with dyes or other specialized reagents (“label-free”). Among advantages, the latter is extremely important as it avoids undesirable interactions between labels and analytes, leading to more reliable and reproducible results. Current solid-state, label-free biosensing techniques such as microarray,⁹ electrochemical-^{10, 11} localized surface plasmon resonance (LSPR)-¹²⁻¹⁴ surface-enhanced Raman scattering (SERS)-^{15, 16} and photonic microring resonator-based¹⁷ microRNA sensors provide good sensitivity. These single-mode detection methods rely on a specific sensing mechanism. For example, LSPR-based methods detect changes in local refractive index of the nanostructures while electrochemical-based measurements detect changes in current. Unfortunately, such changes can also result from non-specific adsorption of endogenous biomolecules from bodily fluids onto the sensor, as well as

1
2
3 structural changes that can be induced following placement within bodily fluids during the
4 measurements. As a result, these techniques suffer from low specificity, particularly when
5 analyzing bodily fluids, and can in turn produce false test results. Further, aside from
6 detecting/analyzing the specific signal change that occurs from the analyte, no additional
7 confirmation of analyte attachment to the sensor can be obtained. Among these techniques,
8 SERS-based biomolecular assays are capable of using Raman signal to provide rich structural
9 information on the analytes. However, current solid-state SERS-based microRNA assays still
10 show many problems, including low sensitivity, poor specificity, and inability to analyze real-life
11 patient samples.^{15, 16, 18-21}

12
13
14
15
16
17
18
19 High specificity is the most crucial factor in creating assays that can avoid false-positive
20 and/or false-negative test results for the POC diagnosis.^{22, 23} To overcome the current
21 technological bottleneck in real-life patient sample analysis, we present, for the first time, the
22 design of a solid-state nanoplasmonic sensor. This novel sensing approach is capable of assaying
23 oncogenic microRNAs directly in human plasma with high sensitivity and specificity. Here, the
24 unique LSPR properties^{24, 25} of noble metal nanoparticles are utilized for the detection of
25 microRNAs via a combined SERS^{26, 27} and plasmon-enhanced fluorescence (PEF)^{28, 29} approach.
26 Importantly, the same nanoplasmonic sensor can be used in this multimodal detection method;
27 no changes to structural parameters are required. To demonstrate the potential translational
28 aspects of our dual detection technique in liquid biopsies for POC diagnosis, we successfully
29 assayed two oncogenic microRNAs (microRNA-10b and microRNA-96). Analysis was
30 performed directly in six bladder cancer patient plasma samples at sub-femtogram/microliter
31 (fg/ μ L) concentrations.
32
33
34
35
36
37
38
39
40
41
42
43
44
45
46
47
48
49
50
51
52
53
54
55
56
57
58
59
60

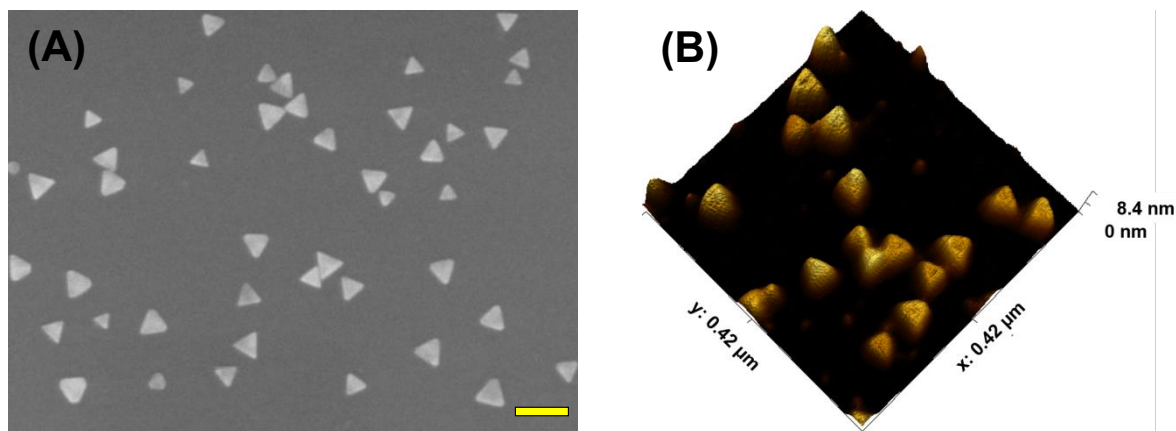


Fig. 1. Structural characterizations of Au TNPs. (A) A representative scanning electron microscopy image of Au TNPs attached onto a silanized glass substrate. Scale bar is 100 nm. (B) An atomic force micrograph of Au TNPs.

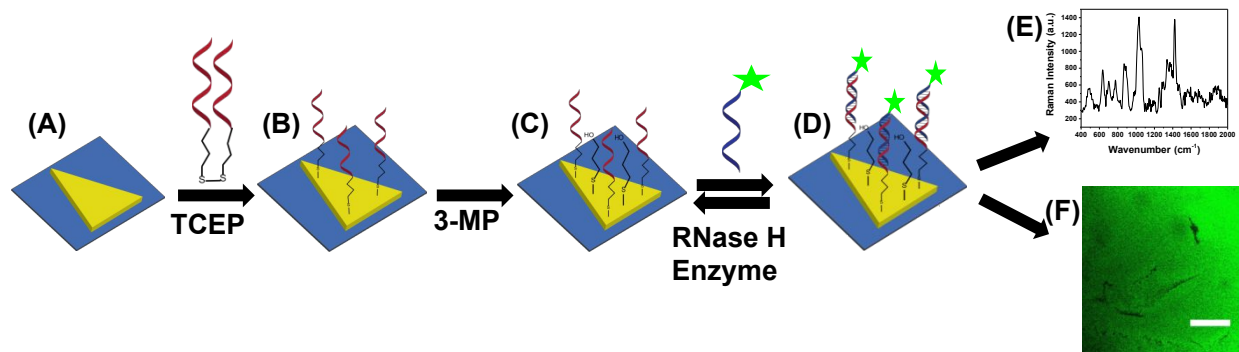


Figure 2. Design of a nanoplasmonic sensor for the detection of microRNAs using combined surface-enhanced Raman spectroscopy (SERS) and fluorescence confocal microscopy techniques. (A) Freshly synthesized Au TNPs were attached onto silanized glass coverslip. (B) Tris(2-carboxyethyl) phosphine (TCEP) addition to DNA-disulfide solution breaks disulfide bonds and subsequent incubation in the solution resulted in the attachment of -ssDNAs on the surface of TNPs. Generally, -ssDNAs were randomly organized on the flat metal surface (e.g., here TNPs).¹⁰ (C) -ssDNA-attached Au TNPs were further functionalized with 3-mercaptopropanol (3-MP) to allow -ssDNAs to “stand up” to achieve the most favorable -ssDNA/microRNA hybridization. The functionalization steps until (C) produced nanoplasmonic sensors, where microRNA-10b/96-FAM can selectively bind (D) to be analyzed by both SERS spectroscopy (E) and fluorescence confocal microscopy (F). Nanoplasmonic sensors can also be regenerated by incubating microRNA-bound sensors in a RNase H enzyme solution; image not to scale.

Experimental Section

Materials. Chloro(triethylphosphine) gold(I) (Et_3PAuCl , 97%) was purchased from Gelest Inc. Poly-(methylhydrosiloxane) (PMHS, $M_n = 1700\text{--}3300$), triethylamine (TEA, 98%), ACS grade acetonitrile (CH_3CN , 99.9%), and 3-mercaptopropanol (3-MP, 95%) were purchased from Sigma-Aldrich. Thiol modified 5'-SH-(CH_2)₃-ssDNAs, and various microRNAs were purchased from Integrated DNA Technologies (IDT). RNase H enzyme and RBS detergent solution were

1
2
3 purchased from Thermo Scientific. (3-Mercaptopropyl)-trimethoxysilane (MPTMS, 94%) was
4 purchased from Alfa Aesar. All the chemicals were used without any further purifications.
5 RNase free sterile water was obtained from Baxter Healthcare Corporation. The glass cover slips
6 and the tris(2-carboxyethyl)phosphine (TCEP) solution were purchased from Fisher Scientific.
7 Bladder cancer patient plasma samples were obtained from the Indiana University medical
8 school and used as received. All water was purified using a Thermo Scientific Barnstead
9 Nanopure system. Thiol modified -ssDNAs, microRNAs were stored at $-80\text{ }^{\circ}\text{C}$. PBS buffer (pH
10 = 7.2) was prepared using RNase-free sterile water. All experiments were performed in
11 accordance with the Guidelines of the United States and approved by the ethics committee at
12 Indiana University. Informed consents were obtained from human participants of this study.
13
14
15
16
17

18
19 **Fabrication of Nanoplasmonic Sensors.** Gold triangular nanoprisms (Au TNPs) were
20 synthesized using our well-established method.^{12, 14, 30} $\text{Et}_3\text{PAu(I)Cl}$ (10 mg) was dissolved in 20
21 mL of acetonitrile. After five minutes of stirring at room temperature, 0.019 mL (0.136 mmol)
22 TEA was added, and the mixture was heated to $40\text{ }^{\circ}\text{C}$. Then, 0.3 mL (2.75 mmol) of PMHS was
23 added, and the reaction ran until the desired LSPR peak of 800 nm was achieved. Au TNPs were
24 then attached onto silanized glass coverslips as we reported previously.¹³ Separately, a mixture
25 of $5\text{ }\mu\text{M}$ -C3-ssDNA-10b/96 with 0.1 M TCEP was prepared and allowed to react for 1 hour to
26 break disulfide bonds. The solution was then diluted with PBS buffer, and the resulting solution
27 was used to incubate Au TNPs for overnight. The addition of -ssDNA-10/96 solutions induced
28 ligand exchange of Au TNPs by removing TEA and PMHS that were present on the surface
29 during the colloidal synthesis. Next, -ssDNA-10b/96-functionalized Au TNPs were washed
30 thoroughly with RNase free water, and both UV-Vis spectrum and Raman spectrum were
31 acquired. Finally, 10 mL, 1.0 mM 3-MP solution was added to ssDNA-10b/96-functionalized Au
32 TNPs to fabricate nanoplasmonic sensors. Various concentrations (100 nM – 100 fM) of
33 microRNA-10b or microRNA-96 in 10 mL PBS buffer were used to incubate nanoplasmonic
34 sensors for 2 hours. MicroRNA bound nanoplasmonic sensors were washed thoroughly with
35 RNase free water to remove any loosely bound microRNAs to the sensor. For the
36 reversibility/regeneration tests, microRNA-bound nanoplasmonic sensors were incubated in 15
37 units RNase H enzyme in RNase free water for 2 hours.
38
39
40
41
42
43
44
45
46
47
48
49
50

51
52 **UV-Vis and SERS measurements, and fluorescence confocal microscopy imaging.** UV-Vis
53 spectra were collected from 1100–300 nm on a Varian Cary 50 UV/Vis spectrophotometer, and
54 all sensors were analyzed in RNase free water. SERS spectra were collected of the sensor on
55
56
57
58
59
60

1
2
3 clean aluminum foil using a Foster-FORAM 785 HP Raman spectrometer with a 785 nm diode
4 laser excitation source. Samples were placed on top of the aluminum foil when analyzed due to
5 the requirement of a clean surface to analyze. The background scan was taken of a polystyrene
6 bead to calibrate the laser. For all SERS measurements, two randomly selected spots were
7 analyzed for each sensor and for three-separate sensors (a total of six measurements). Using a
8 Fluoview FV1000 MPE laser scanning biological microscope, 100 nM Alexa-488 dye was used
9 in the analysis of the sensors. A laser power of 40%, a 60x water objective, and gain of 1x were
10 used for the image acquisition. The diameter of the laser spot was 5- μ M.

11
12 **Scanning Electron and Atomic Force Microscopy Analyses.** The chemically synthesized Au
13 TNPs attached onto the silanized glass coverslips were characterized by scanning electron
14 microscopy (SEM) and atomic force microscopy (AFM). SEM micrographs were obtained using
15 a Hitachi S-4700 Field Emission Scanning Electron Microscope (FESEM) at 20 kV accelerating
16 voltage, and AFM images were obtained using a Bioscope AFM instrument.

17
18 **Construction of Calibration Curves.** All SERS spectra were baseline corrected using OMNIC
19 software. The Fit Peaks tool was used in Origin 2018b to find peak intensity with Lorentz fitting.
20 Peak intensity at a specific wavenumber was graphed as a function of concentration. Linear
21 fitting was used to find the R-squared value.

22
23 **Measuring False Responses.** In order to demonstrate the efficiency of our solid-state
24 nanoplasmonic-based sensors mitigating false responses, we analyzed the patient samples that
25 measured the highest and lowest concentrations. Nanoplasmonic-based sensors, which were
26 used to quantify microRNA-10b/96 in patient plasma again re-incubated in 15 units RNase H
27 enzyme in RNase free water for 2 h. Next, both SERS measurement fluorescence confocal
28 measurements were performed. Again, the same sensors were incubated in a 100 nM solution of
29 microRNA-FAM. After the sensors were thoroughly washed with RNase free water, SERS and
30 fluorescence analyses were conducted.

Results and Discussion

To acquire both SERS and PEF signals from the same nanoplasmonic sensor, we used chemically-synthesized gold triangular nanoprisms (Au TNPs) to generate high intensity LSPR.³¹ This intensified LSPR arises due to strong electromagnetic field (EM) enhancement that occurs at the sharp tips and edges of Au TNPs.³²⁻³⁵ This leads to the formation of hot-spots, which are ideal for LSPR-based SERS and PEF mechanisms.^{26, 29} For the first time, we have utilized PEF to unequivocally confirm microRNA attachment onto the nanoplasmonic sensor by utilizing fluorescence confocal imaging. Together, these methods fully eliminate the possibility of false assay responses. Further, in addition to their unique LSPR properties, the atomically flat Au TNPs allow -ssDNAs to form a tightly-packed self-assembled monolayer (SAM) on their surface, allowing for high reproducibility throughout the sensor. This is important in the context of making good interactions and forming a -ssDNA/microRNA duplex. Moreover, tightly-packed SAMs avoid non-specific adsorption of biomolecules onto the Au surface. Au is also extremely stable in human biofluids, therefore sensors are expected to maintain excellent structural integrity. Taking into consideration all their unique structural properties, we chose to Au TNPs with a 42 and 8 nm edge length and thickness, respectively, for the fabrication of our nanoplasmonic sensors, as shown in **Fig. 1**.

The fabrication of nanoplasmonic sensors is illustrated in **Fig. 2**, where : (A) Au TNPs were chemically-attached onto silanized glass substrate; (B) TNPs were functionalized with -ssDNA-(10b/96) via the Au-S bond, and in order to increase their specificity in SERS, they were further functionalized with 3-mercaptopropyl (3-MP) (**Fig. 2C**) so that the -ssDNA-10b/96 would appear in a “standup” position. This standup formation creates an ideal distance between the fluorophore and Au TNPs to maximize PEF enhancement by reducing fluorescence quenching through the Förster resonance energy transfer (FRET) process. In addition, stand-up -ssDNAs provides adequate space for the microRNAs to form -ssDNA/microRNA duplexes. Finally, 3-MP also improves specificity, as reported in the literature.¹⁰ The functionalizations of Au TNPs with -ssDNA-(10b/96) and 3-MP represent our nanoplasmonic sensors. **Fig. 2D** shows attachment of a fully complementary microRNA tagged with a 6-fluorescein (FAM), allowing complete -ssDNA/microRNA-FAM hybridization. Most importantly, as shown in **Fig. 2D**, the nanoplasmonic sensors are fully reversible and regenerative to allow use for multiple analyses.

1
2
3 This is critical in the context of determining sensor stability and showing that they maintain
4 complete structural integrity during assays.
5
6

7 Attachment of microRNA-FAM to the nanoplasmonic sensor can be detected/confirmed
8 utilizing both SERS (**Fig. 2E**) and fluorescence confocal microscopy (**Fig. 2F**) techniques. It is
9 important to highlight the additional advantages of selecting this particular dimension Au TNP
10 for a SERS-based microRNA assay: (1) As shown in **Fig. S1**, the LSPR peak position of
11 nanoplasmonic sensors is ~ 860 nm. The LSPR peak of TNPs and the wavelength of incident
12 laser light controls the intensity of hot-spots. Ideally, for the EM-field-driven SERS
13 enhancement, the LSPR wavelength of nanostructures in the sensors should be longer than the
14 wavelength of laser light; (2) Use of a low energy laser (e.g., 785 nm) that fits the excitation
15 requirements for nanostructures is important for biosensing applications in order to avoid
16 degradation of biomolecules, particularly microRNAs.
17
18
19
20
21
22
23
24

25 Each step in the fabrication of these nanoplasmonic sensors was characterized through
26 SERS spectroscopy (see **Fig. 3**). Attachment of -ssDNA-(10b/96) via Au-S bonds results in the
27 appearance of a C-S Raman stretch at 635 cm^{-1} . Furthermore, several new Raman stretches that
28 are characteristic of DNAs (see **Fig. 3A and Fig. S2**) such as guanine (G) ring breathing at 688
29 cm^{-1} , adenine ring breathing at 733 cm^{-1} , cytosine ring breathing at 790 cm^{-1} , and the
30 phosphodiester group of the nucleic acids at 1289 cm^{-1} are also observed.^{18, 21, 36-38} The C-H
31 Raman stretch at 1400 cm^{-1} further confirms the functionalization of Au TNPs with 3-MP
32 (Figure 3A-blue).³⁹ Incubation of microRNA-(10b/96)-FAM to the nanoplasmonic sensor
33 displays a prominent Raman peak at 1062 cm^{-1} of the additional PO_2^- symmetrical stretch.³⁸
34 Furthermore, the Raman stretch at 1255 cm^{-1} corresponds to guanine C8-H bending^{18, 21, 36, 37} and
35 the low intensity Raman stretch at 1645 cm^{-1} is unique to the uracil C=O stretch.^{18, 21, 36, 37} **Fig.**
36 **3B** illustrates SERS spectra of the microRNA-10b varying concentrations from 100 nanomolar
37 (nM) to 100 femtomolar (fM).
38
39
40
41
42
43
44
45
46
47

48 The average edge-length of our chemically synthesized Au TNPs is 42 nm that provides a
49 top surface area of 764 nm^2 . Considering all the -ssDNA probes were attached onto the top
50 surface and thiolate has a 0.25 nm^2 footprint, there would be approximately 3000 -ssDNA-
51 (10b/96) attached per TNP. In the nanoplasmonic sensors fabrication, we used a high
52 concentration of 3-MP in comparison to -ssDNA probes. Therefore, the -ssDNA grafting density
53
54
55
56
57
58
59
60

is overestimated because a relatively large percentage of TNP surface would be occupied by 3-MP molecules. Further experimental characterization is required to quantitatively determine the grafting density of -ssDNA probe that is currently under our investigation.

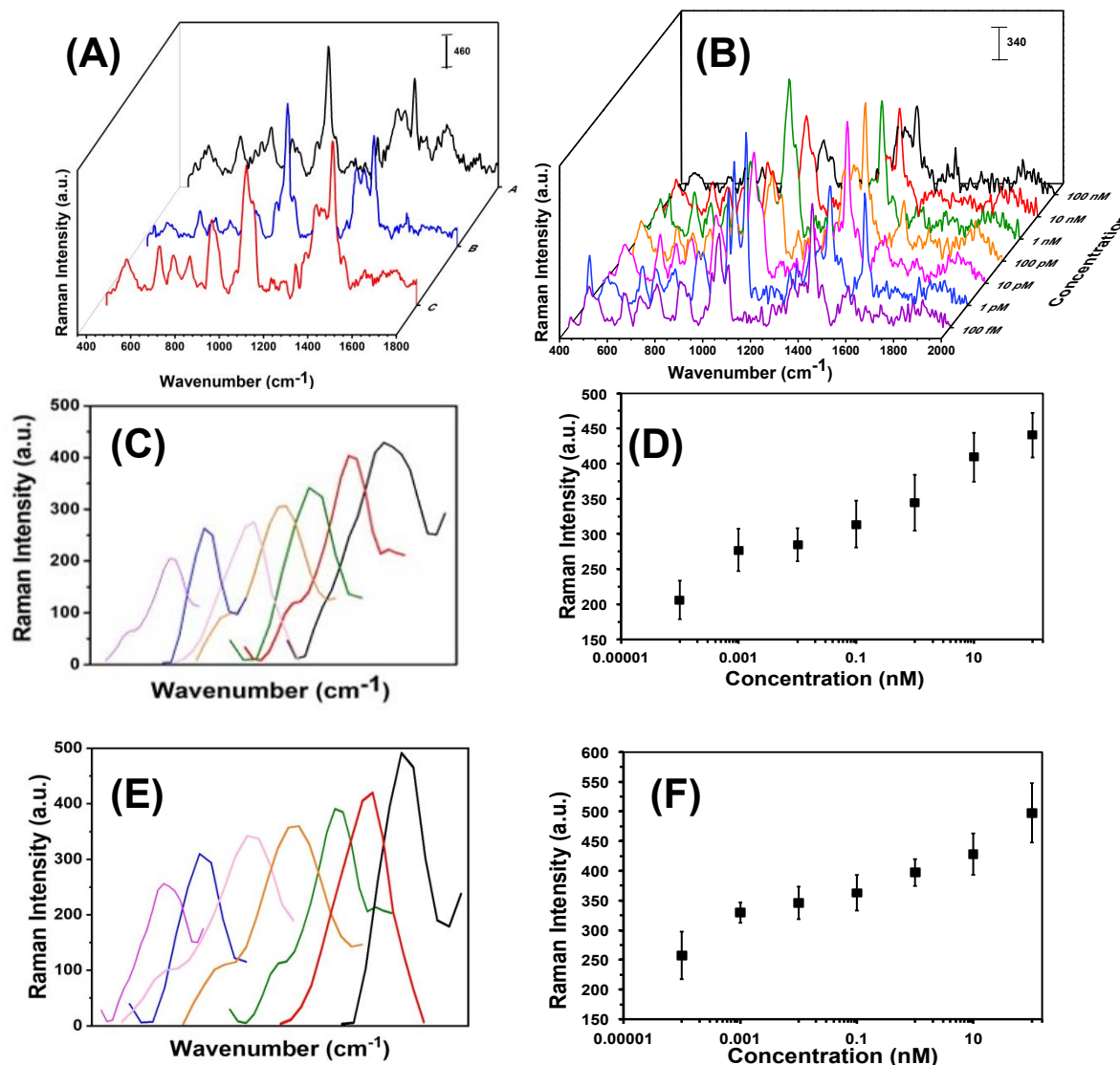


Fig. 3. The SERS-based microRNA assay using nanoplasmonic sensors. (A) SERS spectra at different stages: Functionalization of AuNPs with -ssDNA-10b, A; after attachment of 3-MP on TNPs, B; and after incubation of nanoplasmonic sensors in a microRNA-10b solution, C. **(B)** SERS spectra of nanoplasmonic sensors upon incubation in different concentrations of microRNA-10b solution. **(C)** Expanded SERS spectra of the C8-H bending stretch of Guanine at 1255 cm⁻¹ in various microRNA-10b concentrations (light purple: 100 fM, blue: 1 pM, pink: 10 pM, orange: 100 pM, green: 1 nM, red: 10 nM,

1
2
3 black: 100 nM). **(D)** Intensity of the C8-H bending stretch at 1255 cm⁻¹ as a function of microRNA-10b
4 concentration (logarithmic scale). $Y = 15.94 \ln(X) + 361.88$, $R^2 = 0.97$. **(E)** Expanded SERS spectra of
5 the C8-H bending stretch of Guanine at 1255 cm⁻¹ in various microRNA-96 concentrations (light purple:
6 100 fM, blue: 1 pM, pink: 10 pM, orange: 100 pM, green: 1 nM, red: 10 nM, black: 100 nM). **(F)**
7 Intensity of the C8-H bending stretch at 1255 cm⁻¹ as a function of microRNA-96 concentration
8 (logarithmic scale). $Y = 15.04 \ln(X) + 408.73$, $R^2 = 0.95$. In C and E, the individual concentrations of the
9 microRNA calibration curve are plotted in order to better visualize of the increase in intensity. Each
10 spectrum has the same wavenumber of 1255 cm⁻¹ and does not shift in wavenumber as seen in the figure.
11

12 In literature, researchers have used a variety of SERS stretches to develop the calibration
13 plots for microRNA assays, but have done so without providing any detailed rationale for their
14 selections.^{16, 19, 40} Theoretical calculations show that the C8-H bending Raman stretch of guanine
15 at 1255 cm⁻¹ could be ideal to develop the calibration plot,⁴¹ thus we selected this SERS stretch
16 for our studies. As shown in **Fig. 3C and E** for microRNA-10b and microRNA-96, respectively,
17 a continuous increase in C8-H stretch intensity is displayed when corresponding nanoplasmonic
18 sensors were incubated in various concentrations of microRNA solution. The SERS intensity of
19 the C8-H bending mode versus the concentration of microRNAs is appeared to be linear over the
20 entire concentration range (**Fig. 3D and F, Table S3 and Table S4**). The limit of detections
21 (LODs) for microRNA-10b and microRNA-96 calibration was calculated using a published
22 method that follows:^{40, 42}
23
24
25
26
27
28
29
30

$$\text{LOD} = 10^{3m/k} \text{fM}$$

31
32 Here, m is the relative standard deviation of the blank and k is the slope of the SERS intensity
33 versus microRNA on the concentration curve. Our LODs for microRNA-10b and microRNA-96
34 are calculated at 1.13 pM and 0.030 pM, respectively. Importantly, this represents a 10-fold
35 improved LODs in comparison to previously reported SERS-based microRNA assays.³⁸ We
36 believe that the high SERS sensitivity of our nanoplasmonic sensors is due the intensified
37 hotspots at the sharp tips and edges of the Au TNPs, as previously shown through discrete dipole
38 approximation calculations.³²⁻³⁴
39
40
41
42
43
44
45
46
47
48
49
50
51
52
53
54
55
56
57
58
59
60

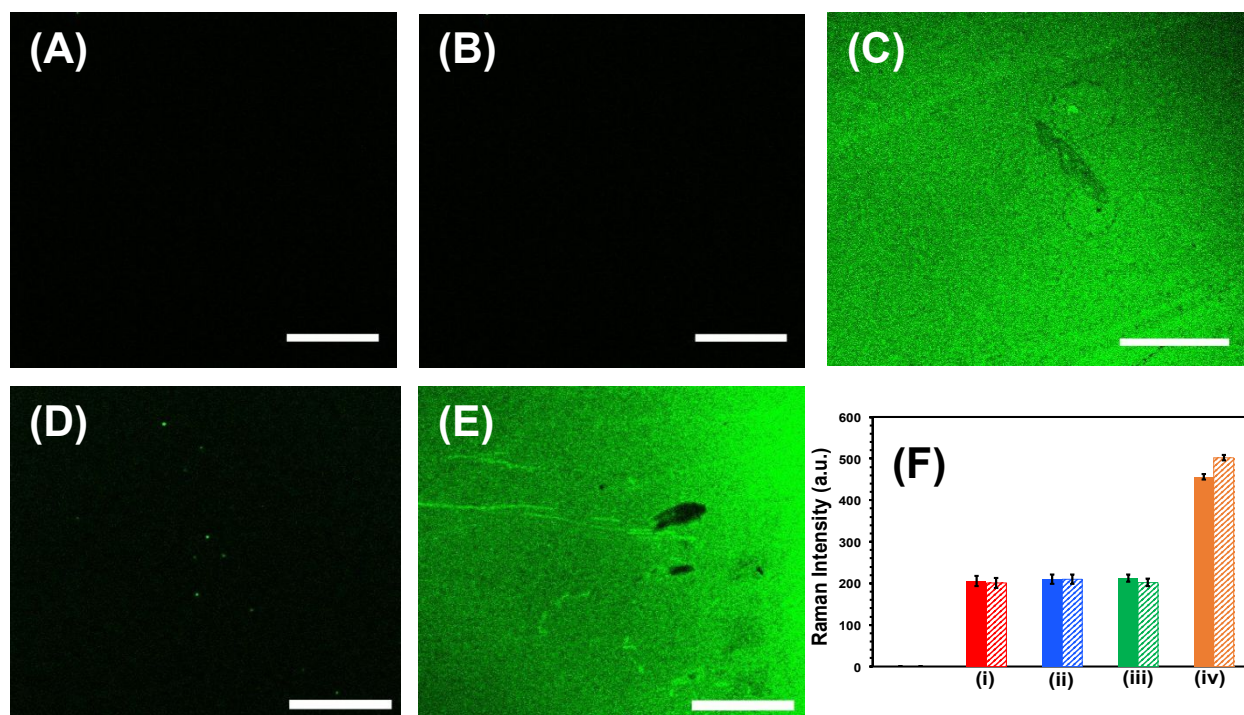


Fig. 4: Specificity tests of nanoplasmonic sensors for the microRNA detection. Fluorescence confocal microscopy images of (A) glass substrate attached Au TNPs, (B) mixed -ssDNA-10b and 3-MP functionalized Au TNPs (nanoplasmonic sensor), (C) After incubation of nanoplasmonic sensors in a 100 nM microRNA-10b-FAM solution, (D) After treatment of nanoplasmonic sensors with RNase H enzyme to regenerate the sensor, (E) After re-incubation of nanoplasmonic sensors in a 100 nM microRNA-10b-FAM solution. Scale bars are 50 μm . (F) Normalized Intensity of the C8-H bending stretch at 1255 cm^{-1} for two different microRNAs (solid bars, microRNA-10b; dashed bars, microRNA-96). Black bars represent glass substrate attached AuNPs (not visible). (i) Red bars represent mixed -ssDNA-10b and 3-MP functionalized Au TNPs or -ssDNA-96 and 3-MP functionalized Au TNPs. (ii) Blue bars represent incubation of nanoplasmonic sensor in a control patient (without the history of cancer) plasma. Green bars represent incubation of nanoplasmonic sensors in a mixture of microRNA-96, 145, 143, and 490-5p solution for the -ssDNA-10b functionalized Au TNPs, or a mixture of microRNA-10b, 145, 143, 490-5p solution for the -ssDNA-96 functionalized Au TNPs. These microRNAs are non-complementary to either -ssDNA-10b or -ssDNA-96. Orange bars represent incubation of nanoplasmonic sensors either in 100 nM microRNA-10b or microRNA-96 solution.

Successful implementation of the developed biosensors in liquid biopsy-based cancer diagnostics requires unprecedentedly high specificity, specifically to avoid false test results.¹ First, the specificity, which is the ability to unambiguously identify the analyte of our nanoplasmonic sensors, was investigated through fluorescence confocal imaging of labeled target microRNAs. We used microRNA-10b as a model system to study the specificity of the nanoplasmonic sensors. **Fig. 4A** confirms that our nanoplasmonic sensors do not display any

1
2
3 fluorescence (in the absence of microRNAs). Similarly, when Au TNPs were functionalized only
4 with 3-MP (without -ssDNA-10b) and then incubated in a microRNA-10b-FAM solution, no
5 fluorescence signals are detected (data not shown). Further, when the 3-MP functionalized Au
6 TNPs were incubated in a -ssDNA-10b solution, no fluorescence is detected (**Fig. 4B**). However,
7
8 when the nanoplasmonic sensors, which were constructed to detect microRNA-10b, were
9
10 incubated in a microRNA-10b-FAM solution followed by copious rinsing, confocal imaging
11
12 shows bright green fluorescence (**Fig. 4C**). Additionally, a control experiment was performed by
13
14 incubating a MPTMS functionalized glass coverslip in -ssDNA and microRNA directly without
15
16 the presence of Au TNPs. The obtained SERS and fluorescence signals showed no results (data
17
18 not shown). These experimental data suggest the formation of a -ssDNA-10b/microRNA-10b-
19
20 FAM duplex. Metallic nanostructures are capable of enhancing fluorescence signal through the
21
22 PEF mechanism, in which LSPR properties of the nanostructure increase the radiative decay rate
23
24 of the fluorophore.⁴³ To reduce fluorescence quenching due to FRET processes between the
25
26 nanostructure and fluorophore, it is important that the fluorophore resides within a particular
27
28 distance from the metal surface. Recent studies showed that a distance of 7.0 to 16.2 nm,
29
30 corresponding to 18 to 45 nucleotides, between Au nanostructures and fluorophores provides the
31
32 strongest fluorescence enhancement.²⁸ Importantly, microRNA-10b contains 23 nucleotides and
33
34 thus the spacing between FAM molecules and Au TNPs is within the reported distance for
35
36 highest fluorescence enhancement. To further confirm our confocal-based imaging results,
37
38 which demonstrate that nanoplasmonic sensors unambiguously detect microRNAs with high
39
40 specificity, we incubated microRNA-10b-FAM-attached nanoplasmonic sensors in a RNase H
41
42 enzyme solution. This solution is expected to break the -ssDNA/microRNA duplex, removing
43
44 the attached microRNA, to regenerate the original sensor. As predicted, following RNase H
45
46 incubation, the fluorescence signal completely disappears, as shown in **Fig. 4D**. As illustrated in
47
48 **Fig. 4E**, the fluorescence signal reappears when sensors were again incubated in then
49
50 microRNA-10b-FAM solution. These results show the fully regenerative capabilities of the
51
52 developed nanoplasmonic sensors. Sensor regeneration was further confirmed by the decrease or
53
54 increase of the 1255 cm⁻¹ peak of the C8-H bending mode in the SERS spectra after -ssDNA-10b
55
56 attachment, 3-MP attachment, microRNA-10b-FAM attachment, incubation in RNase H enzyme,
57
58 and re-incubation in microRNA-10b-FAM (**Fig. S3**).

1
2
3
4
5
6
7
8
9
10
11
12
13
14
15
16
17
18
19
20
21
22
23
24
25
26
27
28
29
30
31
32
33
34

Next, we investigated the specificity of our label-free assay for microRNA-10b and microRNA-96 detection using the SERS technique, as shown in **Fig. 4F** and **Fig. S4**. Here, the nanoplasmonic sensors, which are capable of detecting microRNA-10b, were incubated in a mixture of microRNA-96, microRNA-145, microRNA-143, and microRNA-490-5p. The levels of these microRNAs are commonly altered in patients with a history of bladder cancer.¹³ SERS analysis shows that the intensity of the C8-H bending mode at 1255 cm^{-1} does not increase when compared to the original nanoplasmonic sensors. This is because microRNA-96, microRNA-145, microRNA-143, and microRNA-490-5p are non-complementary to –ssDNA-10b. However, when the same nanoplasmonic sensor was incubated in the complimentary microRNA-10b solution, an increase in SERS intensity of the C8-H bending mode is observed. Thus, by measuring the Raman intensity in the presence of either non-complimentary/complementary microRNAs, we can unequivocally conclude the high specificity of our nanoplasmonic sensors towards targeted microRNAs. Taken together, our multimodal fluorescence and SERS analyses not only confirm the high specificity of the nanoplasmonic sensors towards the microRNA assay, but also demonstrate the reusability of the newly developed label-free technique. Sensor regeneration is a particularly an important aspect as the ability for repeated measurements not only provides unmatched accuracy, but also it is commercially important in low- and middle-income countries.

35
36
37
38
39
40
41
42
43
44
45
46
47
48
49
50
51
52
53
54
55
56
57
58
59
60

To demonstrate the translational aspects of our newly developed technology for clinical POC cancer diagnostics, we successfully assayed two oncogenic microRNAs (microRNA-10b and microRNA-96) directly in plasma from metastatic bladder cancer patients. **Fig. 5A** demonstrates microRNA-10b and microRNA-96 levels in six patients. It should be noted that all patients were categorized in the metastatic stage; however, the level of microRNA varies from one to another. To mitigate false positive and false negative test results, we re-analyzed the two nanoplasmonic sensors that measured the highest (patient 2 shows a high microRNA-10b level that could arise from false positive response) and the lowest (patient 5 shows a low microRNA-10b level that could lead to false negative response) microRNA-10b concentrations. It is expected that both sensors that were incubated in the patient plasma containing – ssDNA/microRNA-10b duplexes. As shown in **Fig. 5B**, SERS intensities decrease following RNase H enzyme treatment. Re-incubation of the regenerated sensors into microRNA-10b-FAM results in nearly the same SERS intensity values, as shown in **Fig. 4F**. Finally, we also

characterized the nanoplasmonic sensor containing microRNA-10b-FAM by fluorescence confocal microscopy, which reveals excellent specificity (**Fig. 5C**). A similar SERS study was also conducted for microRNA-96 involving patient 3 and 6 (see **Fig. 5D**) as described for microRNA-10b.

To the best of our knowledge, this is the first example where a SERS-based technique has been successfully implemented in the microRNA assay of clinically relevant samples without any sample processing. Experimental data confirm that the developed nanoplasmonic sensors did not compromise sensitivity or specificity aspects upon incubation in patient plasma, and the concentrations that were determined are true values.

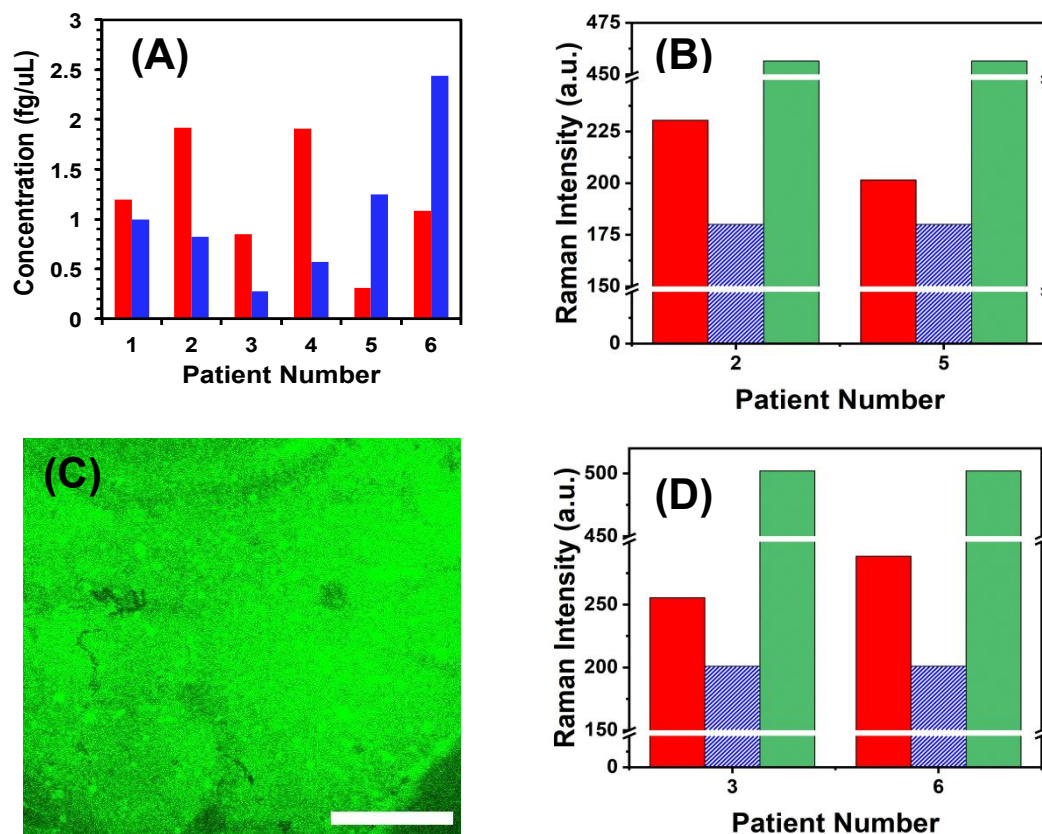


Fig. 5. Nanoplasmonic sensor-based liquid biopsy for cancer detection. (A) SERS-based microRNA quantification in six different bladder cancer-related patient plasma samples. microRNA-10b and microRNA-96 are shown in red and blue bars, respectively. (B) Examination of false test resulting by measuring SERS intensities for two different patients containing the highest (patient 2) and the lowest (patient 5) microRNA-10b levels. Red solid bars represent the Raman intensity of C8-H bending stretch at 1255 cm^{-1} , blue dashed bars after regeneration of nanoplasmonic sensors through RNase H treatment, and green dotted bars are after incubation of nanoplasmonic sensors in 100 nM microRNA-10b-FAM solution. (C) A representative fluorescence confocal image of the nanoplasmonic sensor after incubating

1
2
3 in 100 nM microRNA-10b-FAM solution. **(D)** Examination of false test resulting by measuring SERS
4 intensities for two different patients containing the lowest (patient 3) and the highest (patient 6)
5 microRNA-96 levels. The bars are color coordinated as shown in panel (B). Scale bars is 50 μm .
6
7
8
9
10

11 **Conclusion**

12
13
14 In conclusion, we have designed and fabricated SERS-based, highly sensitive, specific, and
15 regenerative nanoplasmonic sensors for the first time. These sensors were capable of quantifying
16 oncogenic microRNAs at sub-fg/ μL concentrations directly from patient plasma, thus obviating
17 the complications associated with current gold-standard qRT-PCR-based technologies. The
18 unique LSPR properties of Au TNPs were utilized to achieve a combined dual-detection SERS
19 and fluorescence analysis that allows mitigation of false test results. The newly developed,
20 label-free microRNA assay technique has unmatched potential to expand SERS-based biomarker
21 quantification in the early detection of cancers through liquid biopsies. Importantly, this holds
22 promise in advancing POC clinical diagnostics, which could be performed using a
23 handheld/portable Raman instrument. Taken together, we believe our multimodal, innovative
24 detection approach, which has been validated using plasma from bladder cancer patients
25 samples, should also be applicable to other cancers (e.g., colon, breast, prostate, and pancreatic)
26 as well as various diseases (e.g., cardiovascular, Alzheimer, and infectious) that involve
27 circulating nucleic acids (e.g., DNAs, long non-coding RNAs, and microRNAs) as biomarkers.⁸
28
29
30
31
32
33
34
35
36
37
38

39 **Acknowledgements**

40
41 This work is supported by the National Science Foundation, award number CBET-1604617. We
42 thank Dr. Daniel Minner for valuable comments and suggestions. We would like to thank
43 Indiana Clinical and Translational Sciences Institute, which was supported, in parts, by Award
44 Number UL1TR002529 from the National Institutes of Health, National Center for Advancing
45 Translational Sciences, Clinical and Translational Sciences Award.
46
47
48
49

50
51 **Electronic Supplementary Information.** Detailed experimental procedures for Au TNPs
52 synthesis, various spectroscopy and microscopy characterizations, and additional extinction and
53 Raman spectra, and raw Raman data. These materials are available free of charge. (PDF)
54
55
56
57
58
59
60

AUTHOR INFORMATION

Corresponding Author

*Rajesh Sardar; Email: rsardar@iupui.edu

References

1. J. Das and S. O. Kelley, *Angewandte Chemie, International Edition*, 2020, **59**, 2554-2564.
2. D. P. Bartel, *Cell* 2004, **116**, 281-297.
3. A. Esquela-Kerscher and F. J. Slack, *Nature Reviews Cancer*, 2006, **6**, 259-269.
4. D. J. Lockhart and E. A. Winzeler, *Nature*, 2000, **405**, 827-836.
5. J. Lu, G. Getz, E. A. Miska, E. Alvarez-Saavedra, J. Lamb, D. Peck, A. Sweet-Cordero, B. L. Ebert, R. H. Mak, A. A. Ferrando, J. R. Downing, T. Jacks, H. R. Horvitz and T. R. Golub, *Nature* 2005, **435**, 834-838.
6. F. Petrocca and J. Lieberman, *RNA Biology*, 2009, **6**, 335-340.
7. J. Wang, J. Chen and S. Sen, *Journal of Cellular Physiology*, 2016, **231**, 25-30.
8. Z. Jin, D. Geißler, X. Qiu, K. D. Wegner and N. Hildebrandt, *Angewandte Chemie, International Edition*, 2015, **54**, 10024-10029.
9. S. Fang, H. J. Lee, A. W. Wark and R. M. Corn, *Journal of the American Chemical Society*, 2006, **128**, 14044-14046.
10. B. N. Johnson and R. Mutharasan, *Anal. Chem.* , 2012, **84**, 10426-10436.
11. M. Wanunu, T. Dadosh, V. Ray, J. Jin, L. McReynolds and M. Drndić, *Nat. Nanotech.*, 2010, **5**, 807-814.
12. G. K. Joshi, S. Deitz-McElyea, T. Liyanage, K. Lawrence, S. Mali, R. Sardar and M. Korc, *ACS Nano*, 2015, **9**, 11075-11089.
13. T. Liyanage, A. N. Masterson, H. H. Oyem, H. Kaimakliotis, H. Nguyen and R. Sardar, *Anal. Chem.* , 2019, **91**, 1894-1903.
14. G. K. Joshi, S. Deitz-McElyea, M. Johnson, S. Mali, M. Korc and R. Sardar, *Nano Letters*, 2014, **14**, 6955-6963.
15. D. Graham, B. J. Mallinder and W. E. Smith, *Angewandte Chemie, International Edition*, 2000, **39**, 1061-1063.
16. Y. C. Cao, R. Jin and C. A. Mirkin, *Science* 2002, **297**, 1536-1540.
17. A. J. Qavi and R. C. Bailey, *Angewandte Chemie, International Edition*, 2010, **49**, 4608-4611.
18. J. L. Abell, J. M. Garren, J. D. Driskell, R. A. Tripp and Y. Zhao, *Journal of the American Chemical Society*, 2012, **134**, 12889-12892.
19. J. D. Driskell and R. A. Tripp, *Chem. Commun.*, 2010, **46**, 3298-3300.
20. L. Qi, M. Xiao, X. Wang, C. Wang, L. Wang, S. Song, X. Qu, L. Li, J. Shi and H. Pei, *Anal. Chem.*, 2017, **89**, 9850-9856.
21. S. Tian, O. Neumann, M. J. McClain, X. Yang, L. Zhou, C. Zhang, P. Nordlander and N. J. Halas, *Nano Letters*, 2017, **17**, 5071-5077.
22. P. Sandbhor Gaikwad and R. Banerjee, *Analyst*, 2018, **143**, 1326-1348.

23. S. K. Vashist, *Biosensors*, 2017, **7**, 62/61-62/64.
24. K. M. Mayer and J. H. Hafner, *Chem. Rev.*, 2011, **111**, 3828-3857.
25. J. N. Anker, W. P. Hall, O. Lyandres, N. C. Shah, J. Zhao and R. P. Van Duyne, *Nat. Mater.*, 2008, **7**, 442-453.
26. P. L. Stiles, J. A. Dieringer, N. C. Shah and R. P. V. Duyne, *Annu. Rev. Anal. Chem.*, 2008, **1**, 601-626.
27. J. R. Lombardi and R. L. Birke, *J. Chem. Phys.*, 2012, **136**, 144704.
28. Z. Mei and L. Tang, *Anal. Chem.*, 2017, **89**, 633-639.
29. J.-F. Li, C.-Y. Li and R. F. Aroca, *Chem. Soc. Rev.*, 2017, **46**, 3962-3979.
30. G. K. Joshi, K. A. Smith, M. A. Johnson and R. Sardar, *Journal of Physical Chemistry C*, 2013, **117**, 26228-26237.
31. T. Liyanage, M. Nagaraju, M. A. Johnson, B. B. Muhoberac and R. Sardar, *Nano Letters*, 2019, **20**, 192-200.
32. L. Scarabelli, M. Coronado-Puchau, J. J. Giner-Casares, J. Langer and L. M. Liz-Marzán, *ACS Nano*, 2014, **8**, 5833-5842.
33. T. Liyanage, A. Rael, S. Shaffer, S. Zaidi, J. V. Goodpaster and R. Sardar, *Analyst*, 2018, **143**, 2012-2022.
34. G. K. Joshi, S. L. White, M. A. Johnson, R. Sardar and P. K. Jain, *Journal of Physical Chemistry C*, 2016, **120**, 24973-24981.
35. G. K. Joshi, K. N. Blodgett, B. B. Muhoberac, M. A. Johnson, K. A. Smith and R. Sardar, *Nano Letters*, 2014, **14**, 532-540.
36. J. D. Driskell and R. A. Tripp, *Chemical Communications (Cambridge, United Kingdom)*, 2010, **46**, 3298-3300.
37. F. Madzharova, Z. Heiner, M. Guehlke and J. Kneipp, *Journal of Physical Chemistry C*, 2016, **120**, 15415-15423.
38. L. Qi, M. Xiao, X. Wang, C. Wang, L. Wang, S. Song, X. Qu, L. Li, J. Shi and H. Pei, *Analytical Chemistry (Washington, DC, United States)*, 2017, **89**, 9850-9856.
39. B. L. Lambert, Gronert, S., Shurvell, F. H., Lightner, A., D., 2011.
40. Z. Wang, S. Ye, N. Zhang, X. Liu and M. Wang, *Anal. Chem.*, 2019, **91**, 5043-5050.
41. B. Giese and D. McNaughton, *Phys. Chem. Chem. Phys.*, 2002, **4**, 5161-5170.
42. Y. He, X. Yang, R. Yuan and Y. Chai, *Anal. Chem.*, 2017, **89**, 8538-8544.
43. *Principles of fluorescence spectroscopy*, ed. J. Lakowicz, Springer, 3rd edn, 2006.

1
2
3
4
5
6
7
8
9
10
11
12
13
14
15
16
17
18
19
20
21
22
23
24
25
26
27
28
29
30
31
32
33
34
35
36
37
38
39
40
41
42
43
44
45
46
47
48
49
50
51
52
53
54
55
56
57
58
59
60

The Table of Contents Graphic

